Optical Engineering

OpticalEngineering.SPIEDigitalLibrary.org

Contribution study of monogenic wavelets transform to reduce speckle noise in digital speckle pattern interferometry

Sara Zada
Yassine Tounsi
Manoj Kumar
Fernando Mendoza-Santoyo
Abdelkrim Nassim

SPIE.

Sara Zada, Yassine Tounsi, Manoj Kumar, Fernando Mendoza-Santoyo, Abdelkrim Nassim, "Contribution study of monogenic wavelets transform to reduce speckle noise in digital speckle pattern interferometry," *Opt. Eng.* **58**(3), 034109 (2019), doi: 10.1117/1.OE.58.3.034109.

Contribution study of monogenic wavelets transform to reduce speckle noise in digital speckle pattern interferometry

Sara Zada,[a,†] Yassine Tounsi,[a,†] Manoj Kumar,[b,†] Fernando Mendoza-Santoyo,[c] and Abdelkrim Nassim[a,*]
[a]Chouaib Doukkali University, Department of Physics, Sciences Faculty, El Jadida, Morocco
[b]Kobe University, Graduate School of System Informatics, Department of Systems Science, Nada, Kobe, Japan
[c]Centro de Investigaciones en Optica, A.C., Leon, Guanajuato, Mexico

Abstract. Wavelets shrinkage is the most illustrative of wavelets transform for speckle noise reduction. We aim to study the performance of a monogenic wavelet transform to reduce the speckle noise in digital speckle pattern interferometric fringes. The proposed method is implemented on simulated and experimental speckle fringe patterns and its performance is appraised on the basis of peak signal-to-noise ratio (PSNR) and quality index (Q). The ability to reduce the speckle noise by the proposed method is compared with other classical speckle denoising methods. The obtained results corroborate the effectiveness of the proposed method for speckle noise reduction in speckle fringes in terms of PSNR and Q. It is also observed that the method provides better qualitative and quantitative results. Furthermore, the proposed method preserves the edge information of the speckle fringes, a feature that is quantified by the edge preservation index. [DOI: 10.1117/1.OE.58.3.034109]

Keywords: speckle denoising; digital speckle pattern interferometry; Riesz transform; monogenic signal; monogenic wavelets transform.

Paper 181666 received Nov. 21, 2018; accepted for publication Mar. 15, 2019; published online Mar. 26, 2019.

1 Introduction

Digital speckle pattern interferometry (DSPI) has evolved to become one of the most accurate optical technique that is widely used for industrial measurements to study object deformations, vibrations, temperature gradients, material properties, defects, damage assessment,[1–8] among many other applications. It enables the full-field measurement of optical phase variations from the acquisition of speckle patterns. The main challenges in speckle interferometry manifest on phase distribution extraction leading to the direct determination of surface deformation. Furthermore, speckle fringe patterns are characterized by a strong speckle noise.[9] This undesired noise influence on the phase distribution estimation accuracy, and therefore, a denoising scheme is necessary in order to reduce the speckle noise from speckle fringe patterns before data analysis.

Several different denoising methods have been reported so far to reduce speckle noise in DSPI.[10–22] Various approaches for speckle noise reduction including gray-scale modification, frame averaging, low-pass filtering, and short space spectral subtraction image restoration technique have been suggested by Lim and Nawab.[10] Another considerable work by Varman and Wykes[11] presents a demonstration of curve fitting and fast Fourier transform techniques to reduce residual speckle noise. Tang et al.[12] gave an overview about the exploitation of partial differential equations (PDEs) and the anisotropic filter-based method for DSPI fringes denoising. Bernini et al.[13] exploited bidimensional empirical mode decomposition to reduce speckle in DSPI, which gives high- and low-frequency mode called intrinsic mode functions (IMFs): the technique recommends to remove the first IMF that contain speckle noise and then reconstruct others IMFs to obtain despeckled fringe patterns.

Several other filtering methods have been demonstrated for noise reduction, such as Lee's filter[14] based on mean and variance computation; Tomasi and Manduchi[15] presented a bilateral filter, and Frost et al.[16] suggested a filtering method based on local statistical characteristics. Recently, Tounsi et al.[17] reported a detailed study about the performance of a nonlocal means filter and its related kernel-based methods for speckle denoising in DSPI. Further, various studies have exploited wavelets transform for speckle noise reduction.[18–22] In Ref. 18, the wavelets transform showed its ability to reduce speckle noise in DSPI fringes and preserve the fringe quality. In the wavelets domain, the thresholding technique was proposed by Shaker et al.[19] They investigated symlet wavelets to enhance DSPI fringes. Barj et al.[20] suggested the stationary wavelets transform thresholding technique, whereas Tounsi et al.[21] proposed the Riesz wavelets transform thresholding technique. Kaufmann and Galizzi[22] proposed a wavelet method based on the thresholding of the wavelet coefficients of the transformed image to reduce speckle noise in synthetic aperture radar images.

Memmolo et al.[23] proposed sparsity denoising of digital holograms speckle noise reduction method, which does not require any prior knowledge of the statistics of the noise. The performances of different speckle noise reduction algorithms digital holographic phase imaging are reported by Montresor and Picart.[24] An improved variational mode decomposition

*Address all correspondence to Abdelkrim Nassim, E-mail: nassim.a@ucd.ac.ma

†These authors contributed equally to this work.

0091-3286/2019/$25.00 © 2019 SPIE

for speckle noise reduction in the DSPI phase map is demonstrated by Xiao et al.[25] In this method, the noisy phase map is decomposed into mode components, and then, according to the mode components characteristics, an adaptive mode threshold method is adopted to process the mode components. Finally, the denoised mode components are reconstructed to obtain the noise-free DSPI phase map.

The purpose of this paper is to study the performance of nonredundant monogenic wavelets transform introduced recently by Unser et al.[26] for speckle denoising in DSPI fringes. In what follows and to begin with, we provide a brief overview of monogenic wavelets transform by presenting monogenic signal theory based on Riesz transform and wavelets analysis; then we explain the monogenic wavelets algorithm for speckle noise reduction; and finally, we present the results obtained using numerical and experimental DSPI data.

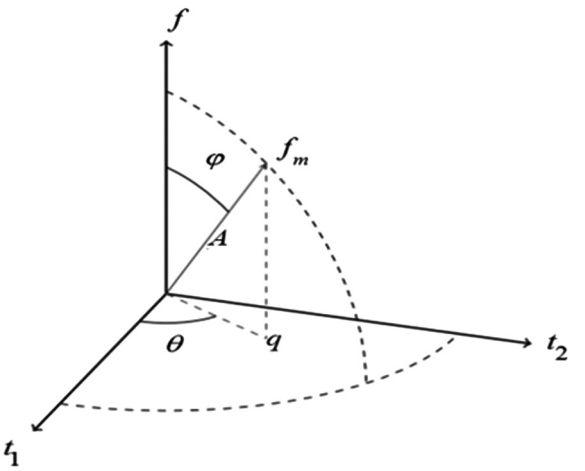

Fig. 1 Geometric representation of the monogenic signal.

2 Monogenic Wavelets Algorithm Description

2.1 *Riesz Transform*

The Riesz transform is the extension of the Hilbert transform for higher dimensions.[27] The impulse responses of n'th-order complex Riesz operator are defined in spatial representation as[28]

$$r^n(x,y) = ni^n(x+iy)^n/2\pi(x^2+y^2)^{n+2/2}, \tag{1}$$

where (x,y) is the spatial coordinate position, n refers to the order of the Riesz operator, and i is the square root of -1. Therefore, the first-order two-dimensional (2-D)-Riesz kernels along x and y directions are expressed as

$$r_x = x/2\pi(x^2+y^2)^{3/2}, \quad r_y = y/2\pi(x^2+y^2)^{3/2}. \tag{2}$$

The application of the first-order Riesz transform to an image $f(x,y)$ gives two components t_1 and t_2 defined as

$$t_1 = r_x * f(x,y); \quad t_2 = r_y * f(x,y), \tag{3}$$

where $*$ refers to the convolution product.

2.2 *Monogenic Signal*

The monogenic signal was introduced by Filsberg and Sommer and is defined as the multidimensional extension of the analytic signal introduced by Gabor.[29] According to Filsberg and Sommer,[30] the monogenic signal for any 2-D intensity distribution $f(x,y)$ is defined as the linear combination of $f(x,y)$ and its Riesz components along the x and y directions.[30,31] Mathematically, the monogenic signal of image $f(x,y)$ is expressed as

$$f_m = f + it_1 + jt_2, \tag{4}$$

where f_m is the monogenic signal of $f(x,y)$, t_1 and t_2 are the Riesz components of $f(x,y)$ and i, j are the complex units with $i^2 = j^2 = -1$. Geometrically, the monogenic signal of $f(x,y)$ noted as f_m is a vector represented in a Cartesian coordinate system illustrated in Fig. 1.

The conversion to spherical coordinates results in the appearance of three essential image related parameters, viz., local amplitude $A(x,y)$, local phase $\varphi(x,y)$, and local orientation $\theta(x,y)$, so that the components of the monogenic signal can be rewritten as

$$f = A\cos\varphi; \quad t_1 = A\sin\varphi\cos\theta; \quad t_2 = A\sin\varphi\sin\theta. \tag{5}$$

From this equation, the three parameters can be computed easily as

$$\begin{cases} A(x,y) = \sqrt{f^2+t_1^2+t_2^2} \\ \varphi(x,y) = a\tan 2\left(\sqrt{t_1^2+t_2^2}/f\right) \\ \theta(x,y) = a\tan 2(t_1/t_2). \end{cases} \tag{6}$$

2.3 *Monogenic Wavelets Transform*

A nonredundant monogenic wavelets transform was introduced by Unser et al.[26] It is based on the computation of Riesz wavelets; as the definition of the monogenic signal, monogenic wavelets are the linear combination between wavelets coefficients and their Riesz transform along the x and y directions. Considering the analysis wavelet $\psi_{s,k}$, we have the wavelets coefficients at each scale expressed as

$$c_s(k) = \langle f, \psi_{s,k}\rangle, \tag{7}$$

and its Riesz transform of order one is computed as

$$c_s^R(k) = \langle f, R^{-1}\psi_{s,k}\rangle = \langle Rf, \psi_{s,k}\rangle = [R(\psi_s * f)], \tag{8}$$

where R is the Riesz operator. The combination between multiresolution aspect is given by the wavelets and the monogenic signal perform a called multiresolution monogenic signal defined as[26]

$$f_{m,s} = (\psi_s * f) + i[R_x(\psi_s * f)] + j[R_y(\psi_s * f)], \tag{9}$$

$$f_{m,s} = c_s(k) + it_{x,s}(k) + jt_{y,s}(k). \tag{10}$$

Using the anisotropic mother wavelet, the monogenic wavelet decomposition of an image gives two sub-bands, such an approximation and details defined as follows:

$$\begin{cases} h_{s,k} = \langle f, \psi_{s,k} \rangle = (\psi_s * f)[2^{-(s+1)k}] \\ g_{s,k} = \langle f, R\psi_{s,k} \rangle = \{R(\psi_s * f)\}[2^{-(s+1)k}] \end{cases}, \tag{11}$$

where $h_{s,k}$ and $g_{s,k}$ are the approximation and details coefficients at scale s, respectively.

The main feature of the monogenic wavelets decomposition is that it gives three monogenic components at each scale/location index. The fact that the Riesz transform is steerable[28] and the necessity of anisotropic mother wavelets make the monogenic wavelet analysis an essential rotation invariant.

The three monogenic wavelets components defined in Eq. (9) give access to the local orientation, local amplitude, and local phase at each scale/location index. These parameters are specific to the monogenic formalism and are not accessible in a conventional wavelet transform. The wavelet domain amplitude, local phase, and orientation are, respectively, computed as

$$\begin{cases} A_s(k) = [c_s(k) + t_{x,s}(k) + t_{y,s}(k)]^{1/2} \\ \varphi_s(k) = \arctan\left[\sqrt{t_{x,s}(k) + t_{y,s}(k)}, c_s(k)\right] \\ \theta_s(k) = \arctan[t_{y,s}(k), t_{x,s}(k)]. \end{cases} \tag{12}$$

2.4 *Monogenic Denoising Algorithm*

The monogenic wavelet analysis contains decomposition of an input image and reconstruction or synthesis of selected monogenic wavelets. Two perfect reconstruction filter banks are used separately in parallel: polyharmonic wavelets and Riesz wavelets transform.[26] Figure 2 shows a block diagram of monogenic wavelets analysis/synthesis of an input image.

At the decomposition stage, a low- and high-pass filtering with downsampling with a factor of two are applied to the input image. From the obtained monogenic wavelets coefficients [approximation and details defined in Eq. (11)], local amplitude, local phase, and local orientation defined in Eq. (12) are computed at each scale. Figure 3 shows the monogenic information computed at scale 1, 2, and 3 of an input speckled fringe patterns.

It is clear that the three multiscale information is influenced by residual speckle noise. In general, speckle noise of DSPI fringes is modeled as multiplicative noise. After applying the monogenic wavelets to the input image, the obtained monogenic wavelets coefficients are selected by their amplitude and thresholded using an appropriate soft thresholding technique.[22] The coefficients characterized by low amplitude are replaced by zeros, then the processed coefficients undergo to a reconstruction step, at this stage, a regression module which produces a critically sampled output, low- and high-pass filtering with upsampling by a factor of two are applied and given in output denoised speckle fringes pattern.

3 Results

3.1 *Numerical Simulation*

The effectiveness of the proposed monogenic wavelet transform (MWT) was first tested using computer-simulated speckle fringes with size 256×256 pixels containing 256 gray levels and a speckle size of 2 pixels. We evaluated the

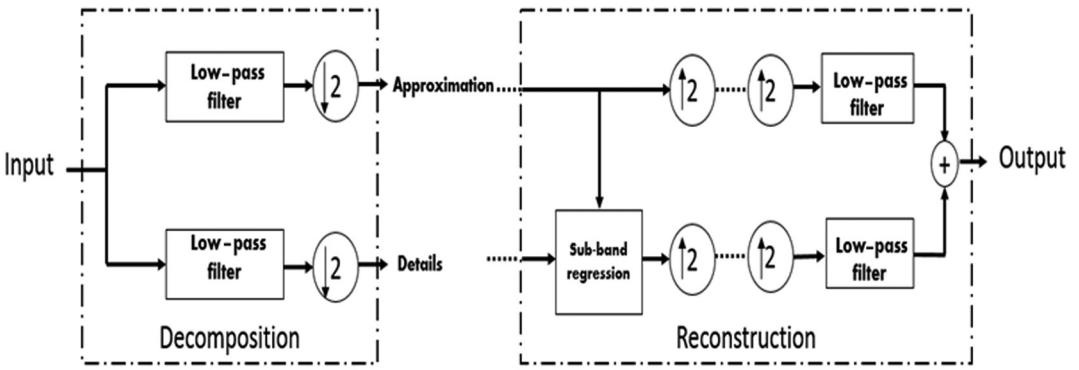

Fig. 2 Block diagram of monogenic wavelets transform analysis/synthesis.

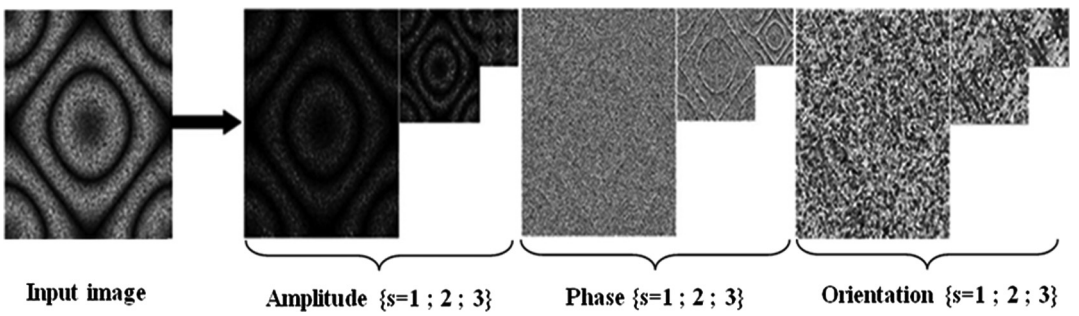

Fig. 3 Monogenic filter bank output (local amplitude, local phase, and local orientation) of speckle fringes.

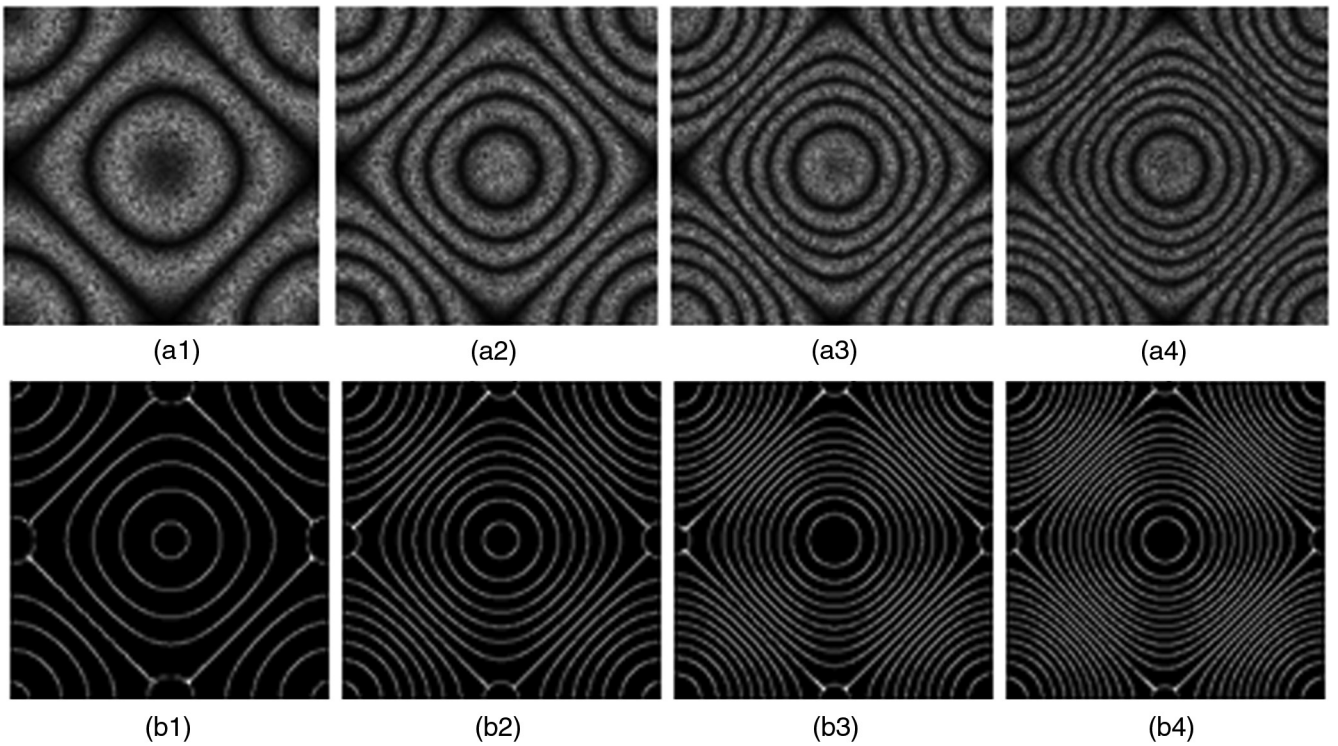

Fig. 4 Computer-simulated speckle fringes with different fringes densities and corresponding theoretical edge maps.

performance of MWT algorithm when fringe densities increase and for wavelets scale decomposition $s \in \{1;2;3\}$. Figure 4 represents the simulated speckle fringe patterns with different fringe densities and their corresponding edge maps. The filtering results on the simulated speckle fringes obtained by the proposed MWT technique are shown in Fig. 5.

We compared the performance of the proposed MWT technique for speckle noise reduction with other filtering techniques such as Lee filter,[14] bilateral filter,[15] Frost filter,[16] and stationary wavelet transform (SWT).[20] Figures 6–9 present, respectively, the filtered speckled fringe patterns by SWT, bilateral filter, Frost filter, Lee filter, and the corresponding edge maps.

3.2 *Performance Study*

The effectiveness of MWT is evaluated using peak to signal noise ratio (PSNR), image quality index (Q), and the edge preservation index (EPI).

3.2.1 *Peak to signal noise ratio*

The PSNR is defined as the ratio between the maximum possible power of a signal and the power of filtered noise and is given by[32]

$$\mathrm{PSNR}(f_{\mathrm{out}}, f) = 10\log_{10}\left[\frac{L^2}{\mathrm{MSE}(f_{\mathrm{out}}, f)}\right], \tag{13}$$

where $L = 2^8 - 1 = 255$ is the maximum possible value of the image pixels when pixels are represented using 8-bits per sample; and $\mathrm{MSE}(f_{\mathrm{out}}, f)$ represents the mean square error between noised and denoised speckled fringe pattern defined as

$$\mathrm{MSE}(f_{\mathrm{out}}, f) = \frac{1}{N.M}\sum_{i=1}^{N}\sum_{j=1}^{M}[f(i,j) - f_{\mathrm{out}}(i,j)], \tag{14}$$

where f is the original image value at pixel (i, j), f_{out} is the denoised image, and M, N represents the image size.

3.2.2 *Image quality index (Q)*

As a comparison method, we use a well-established image quality index Q calculation.[32,33] It is defined as

$$Q = \frac{4\sigma_{xy}\langle f\rangle\langle f_{\mathrm{out}}\rangle}{(\sigma_x^2 + \sigma_y^2)[(\langle f\rangle)^2 + (\langle f_{\mathrm{out}}\rangle)^2]}, \tag{15}$$

where $\langle f\rangle$ and $\langle f_{\mathrm{out}}\rangle$ represents, respectively, the average of the speckled and despeckled image; and σ_x and σ_y are the standard deviation of the two images, respectively. The Q index is calculated locally using an 8×8 sliding window and averaged to obtain a single value from the range $(-1,1)$, with 1 corresponding to the perfect match.

3.2.3 *Edge preservation index*

The EPI corresponds to the edge saving capability of filters. It is defined as

$$\mathrm{EPI} = \frac{\sum_{i=1}^{m}\sum_{j=1}^{n-1}|f_{\mathrm{out}}(i,j+1) - f_{\mathrm{out}}(i,j)|}{\sum_{i=1}^{m}\sum_{j=1}^{n-1}|f(i,j+1) - f(i,j)|}, \tag{16}$$

where f_{out} and f represent, respectively, denoised and original images. The higher value of EPI means better edge

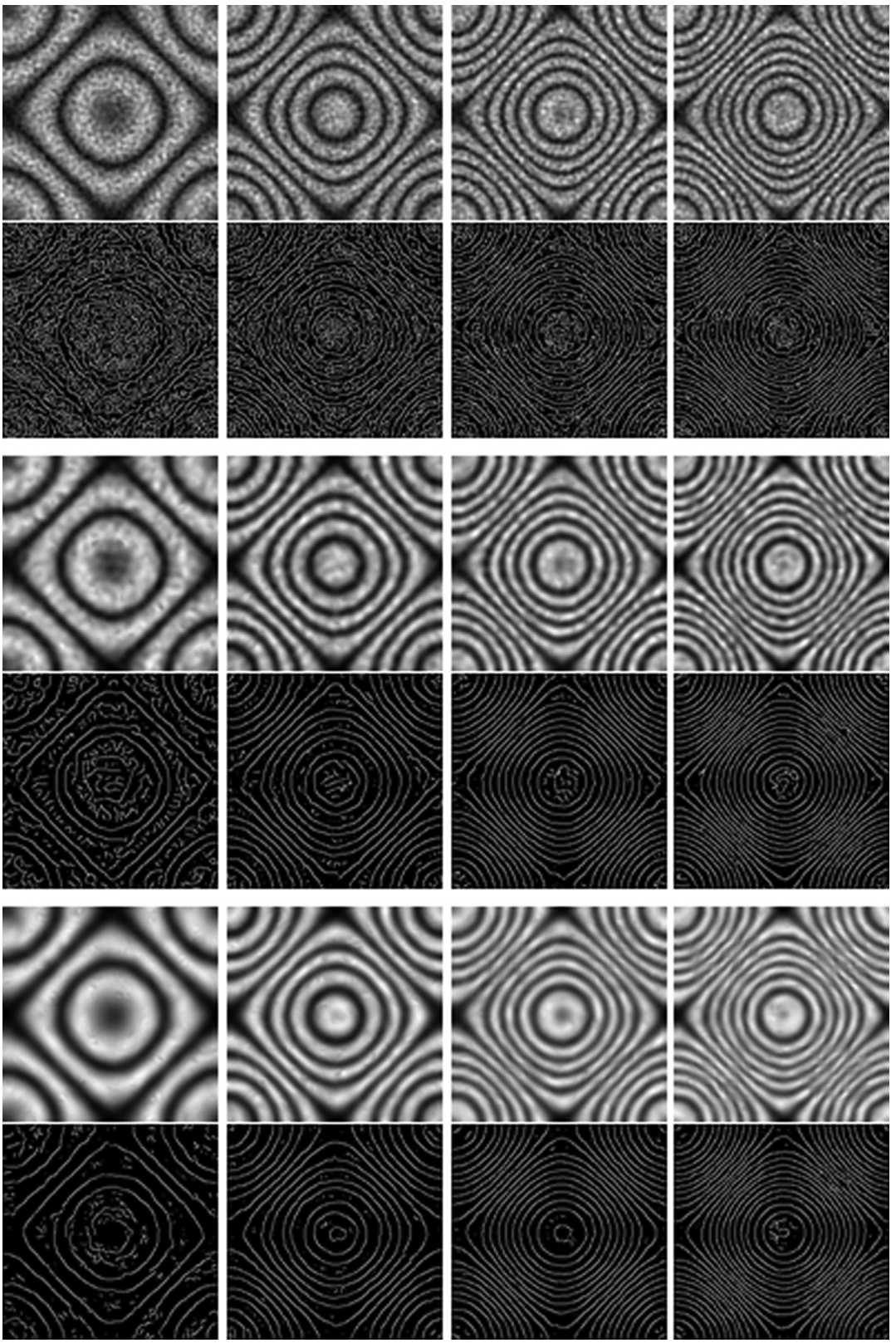

Fig. 5 Denoised speckle fringes and corresponding edge maps for Riesz order ($n = 1$) and scale decomposition $s = 1$ (rows 1, 2); $s = 2$ (rows 3, 4); and $s = 3$ (rows 5, 6).

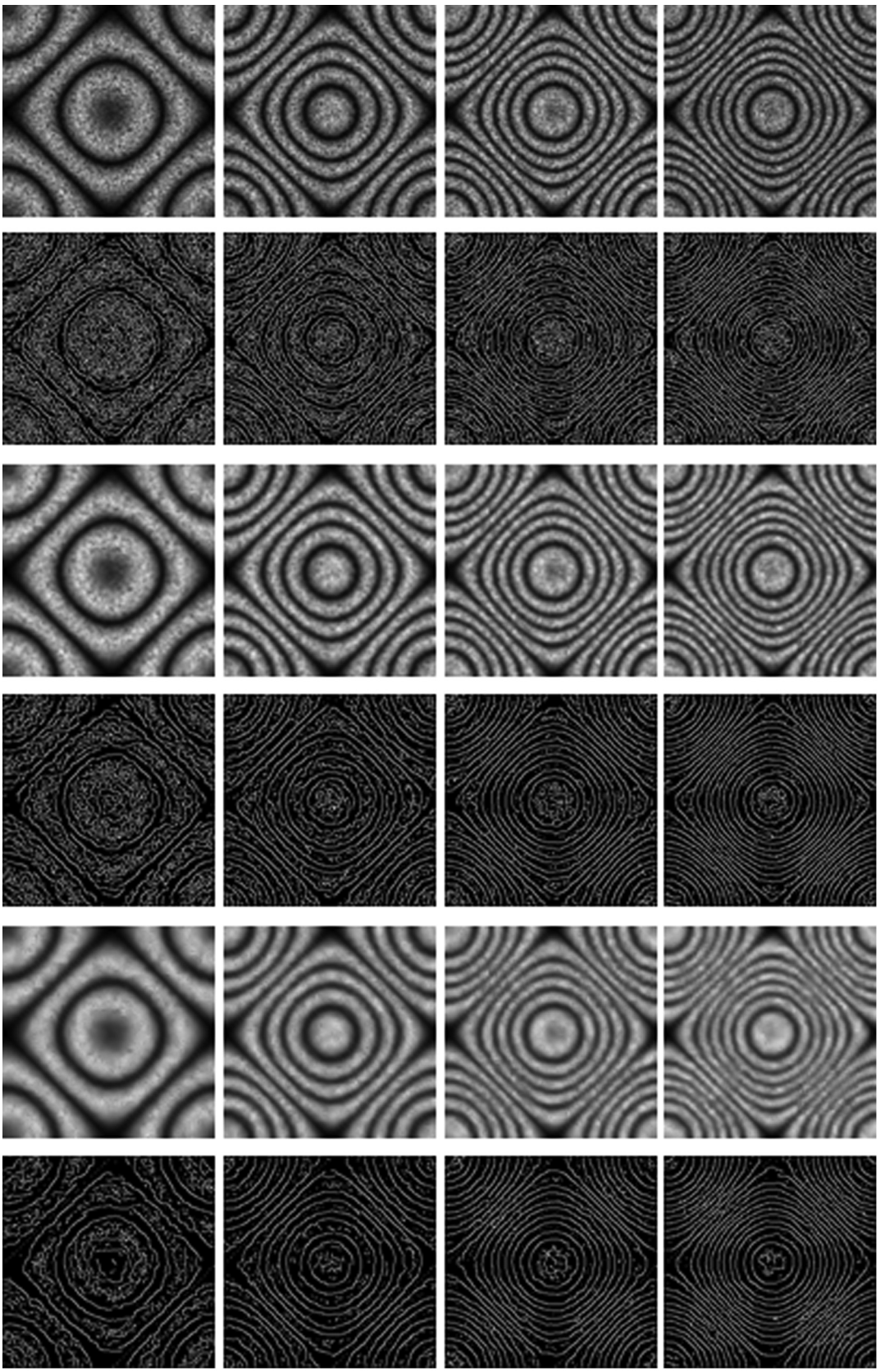

Fig. 6 Denoised speckle fringes by SWT and corresponding edge maps for scale decomposition $s = 1$ (rows 1, 2); $s = 2$ (rows 3, 4); and $s = 3$ (rows 5, 6).

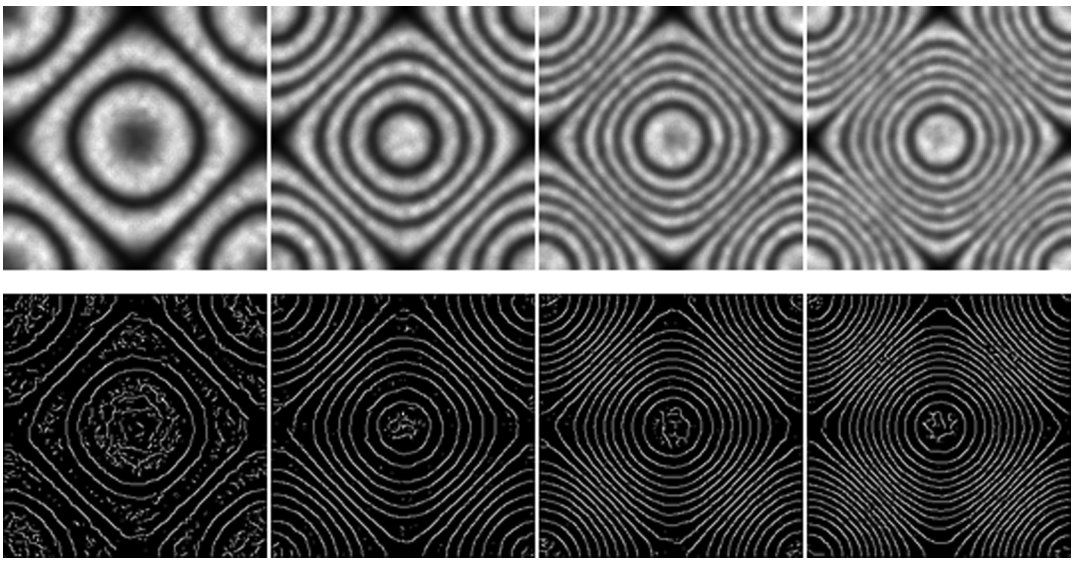

Fig. 7 Denoised speckle fringes by the bilateral filter and corresponding edge maps.

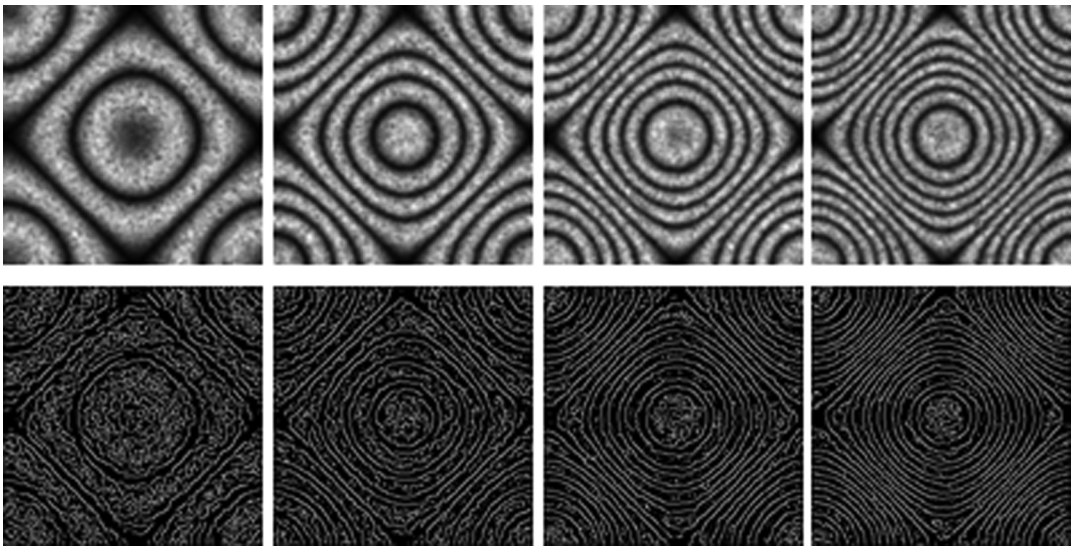

Fig. 8 Denoised speckle fringes by Frost filter and corresponding edge maps.

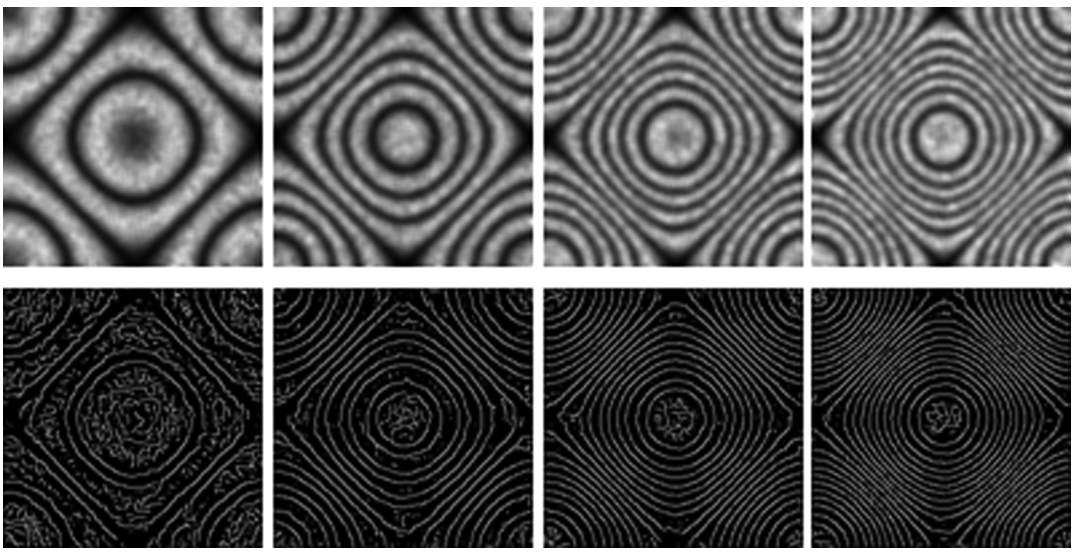

Fig. 9 Denoised speckle fringes by Lee filter and corresponding edge maps.

preservation. Table 1 provides the obtained three metric values computed between clean fringe patterns and denoised speckled fringe pattern.

According to Table 1, it is observed that the proposed technique provides good results at scale 3 in terms of PSNR, Q, and EPI despite the fact that the fringe density increases. The main objective of speckle denoising is improving phase distribution. Figure 10 shows phase demodulation at scale 1, 2, and 3 before and after denoising of speckle fringe pattern presented in Fig. 3(a1).

Further, the performance of the MWT technique for different speckle sizes (4, 3, 2.5, and 1) is also evaluated. Figure 11 presents some simulated DSPI fringes with different speckle size and their corresponding denoised DSPI fringes by the proposed technique. The denoised DSPI fringes for different speckle sizes by the proposed technique reveals that the proposed technique effectively denoise the DSPI fringes and provides promising results as the speckle size increases, which is evaluated on the basis of PSNR, Q, and EPI. The calculated values of (PSNR, Q, EPI) for the denoised DSPI fringes shown in Figs. 11(e)–11(h) are (18.1253, 0.69, 0.89); (28.2395, 0.78, 0.97); (36.9561, 0.787, 0.94); and (37.2510, 0.798, 0.96), respectively.

3.3 *Experimental Results*

In order to illustrate the performance of the speckle noise reduction by monogenic wavelet, the algorithm was implemented on various experimental speckled fringe patterns recorded by the optical setup shown in Fig. 12.

In this experimental setup, a 15-mW He–Ne laser is used as the light source. The laser beam is split into reference and object beams by a beam splitter (BS1). The beam expander directs the object beam to illuminate the object surface under study and due to its roughness produces the speckle field. The speckled image of the object is formed on the camera sensor with the help of the imaging lens L. The reference beam is spatially filtered by a spatial filter and collimated with lens (C) and then interferes with the object beam via the beam combiner (BS2), on the camera sensor. The interference of the object and reference beams forms a speckleogram, which is recorded by the sensor, with 640 pixels ×

Table 1 Performance of MWT and other techniques for speckle reducing in terms of PSNR, Q, and EPI for different speckle fringe densities shown in Fig. 3.

		Fig. 3(a1)			Fig. 3(a2)			Fig. 3(a3)			Fig. 3(a4)		
Filtering techniques		PSNR	Q	EPI	PSNR	Q	EPI	PSNR	Q	EPI	PSNR	Q	EPI
Monogenic wavelets transform	$s=1$	28.3256	0.6823	0.9218	27.2384	0.6711	0.9101	27.4256	0.6722	0.8979	27.3298	0.6692	0.8946
	$s=2$	32.5896	0.7123	0.9293	32.5126	0.7120	0.9216	32.1542	0.71098	0.9145	31.9526	0.71050	0.9056
	$s=3$	37.9961	0.7879	0.9516	37.9961	0.7879	0.9448	37.9961	0.7879	0.9426	37.9961	0.7879	0.9414
Stationary wavelets transform	$s=1$	32.0708	0.7570	0.9208	32.1205	0.7565	0.9224	32.0325	0.7511	0.9207	31.2518	0.7510	0.9314
	$s=2$	36.2873	0.7691	0.9285	36.1284	0.7611	0.9215	31.5849	0.7634	0.9236	32.5813	0.7545	0.9363
	$s=3$	36.8727	0.7716	0.9536	36.6953	0.7698	0.9428	31.8506	0.7681	0.9418	31.9526	0.7413	0.9400
Bilateral filter		39.4602	0.7502	0.9206	39.4602	0.7502	0.9206	39.4602	0.7502	0.9206	39.4602	0.7502	0.9206
Lee filter		37.9395	0.7812	0.9352	37.9395	0.7812	0.9345	37.9395	0.7812	0.9348	37.9395	0.7812	0.9355
Frost filter		30.3516	0.7532	0.9422	30.6520	0.7511	0.9411	30.2106	0.7498	0.9399	30.1128	0.7458	0.9354

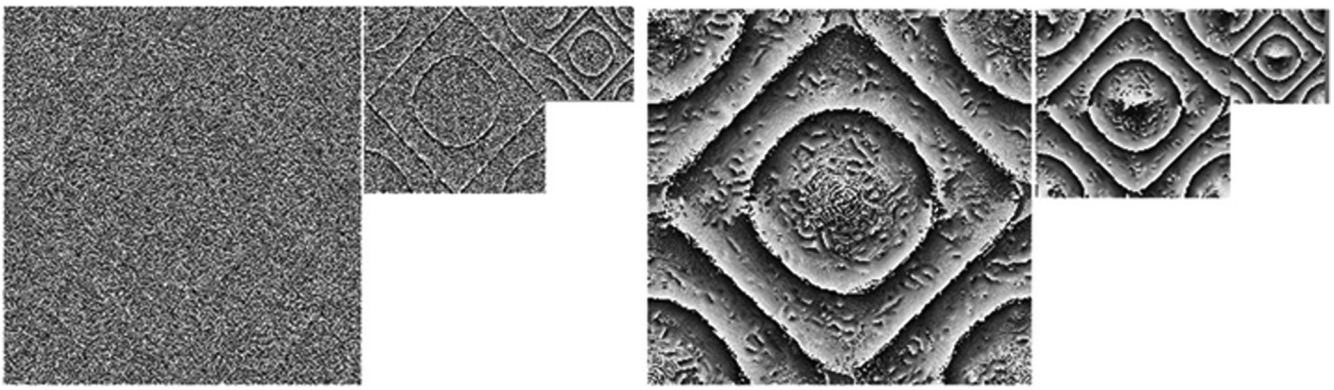

Fig. 10 Phase distribution of speckle fringes before (a) and after (b) denoising by MWT.

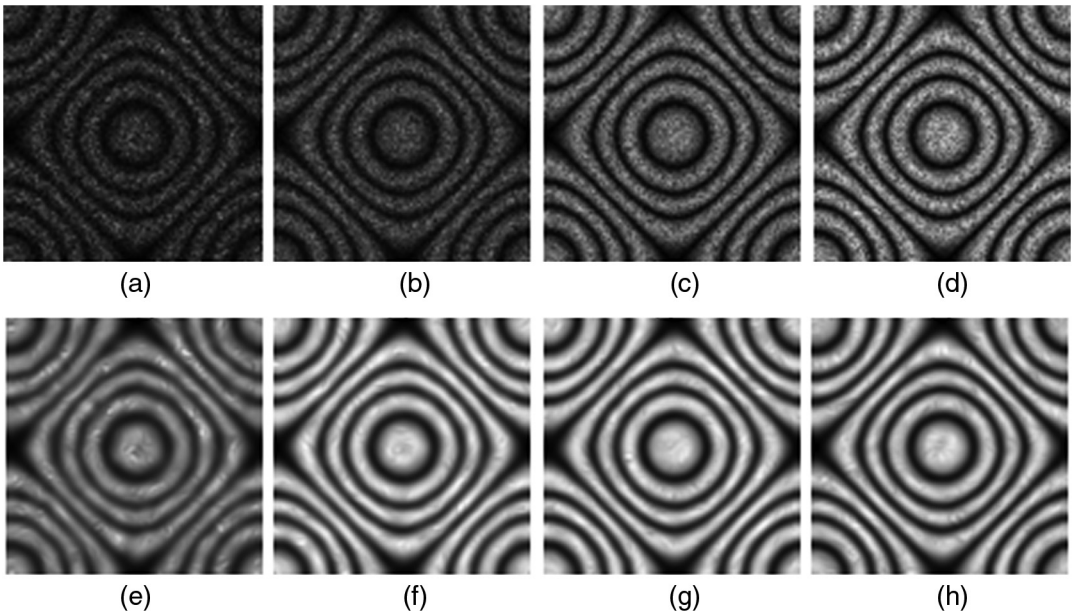

Fig. 11 Speckle size effect study. Row 1 (a)–(d) simulated DSPI fringes with different speckle sizes = 4, 3, 2.5, and 1, respectively. Row 2 (e)–(h) corresponding denoising DSPI fringes by MWT technique.

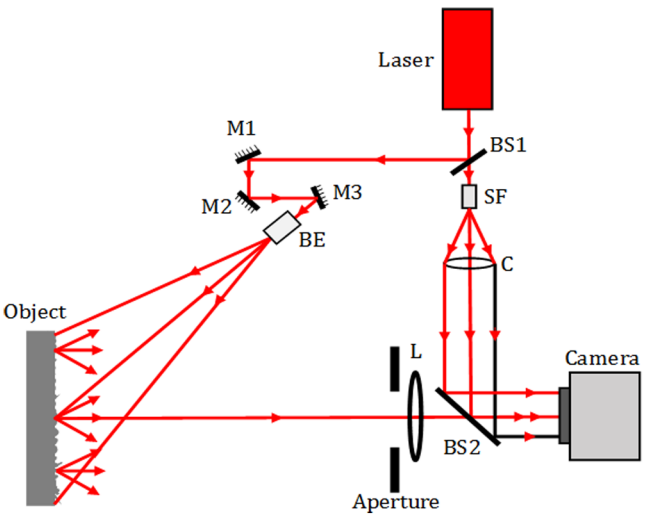

Fig. 12 Schematic experimental setup of DSPI.[17]

640 pixels; pixel size—9 μm, at the 8-bit dynamic range. In DSPI, two specklegrams corresponding to the two different states of the object are recorded. These two specklegrams are then subtracted to obtain the speckle fringes. Figures 13(a) and 13(b) show typical DSPI fringes and Figs. 13(c) and 13(d) show the normalized intensity profile plotted along the white line corresponding to Figs. 13(a) and 13(b), respectively. Figures 13(e) and 13(f) show the filtered DSPI fringes by the proposed method, whereas Figs. 13(g) and 13(h) show their normalized intensity profiles.

The performance of MWT to denoise real DSPI fringes is evaluated using the signal-to-noise ratio (SNR). This metric is defined as the ratio of the mean to the deviation of the denoised DSPI fringes. It compares the level of the desired image to the level of background noise. The higher the ratio is, the less obtrusive the background noise is. The obtained SNR values are 20.23 for Fig. 13(e) and 20.48 for Fig. 13(f).

4 Conclusion

The objective of this work is to study the contribution of nonredundant MWT in the field of residual speckle noise reduction. After monogenic wavelets decomposition of the speckle fringe (DSPI fringe pattern), the obtained wavelets amplitude coefficients undergo to thresholding technique, and then the new coefficients are synthesized in order to get the output denoised fringes. The obtained results are analyzed on the basis of several image quality assessment metrics such as PSNR, quality index (Q), and EPI. These matrices evaluate the quality of the processed DSPI fringes and the calculated values of these matrices reveal that MWT is able to reduce the residual speckle noise effectively from DSPI fringes. Moreover, the proposed speckle noise reduction method provides better results in comparison with other technique such as stationary wavelets transform, bilateral filter, Lee filter, and Frost filter, evaluated on the basis of these metrics and presented in Table 1. A close examination on the metric values obtained for proposed and the other aforementioned filtering methods accommodated that the proposed filtering method provides promising and more pleasing results, e.g., the PSNR, Q, and EPI values for the filtered DSPI fringe pattern, shown in Fig. 3(a1), are higher in comparison to other filtering results performed on the same DSPI fringe pattern. However, the bilateral filter provides better PSNR value but at the cost of lower image quality (Q) and edge-preserving details (EPI) at the same time. A similar trend is observed for the DSPI fringe pattern with increased fringe density; however, the metric values also decrease for the obvious reasons. Finally, it is demonstrated that the application of the proposed MWT filtering method in reducing speckle noise from the experimentally obtained DSPI fringes also provides favorable results, which are evaluated on the basis of SNR values.

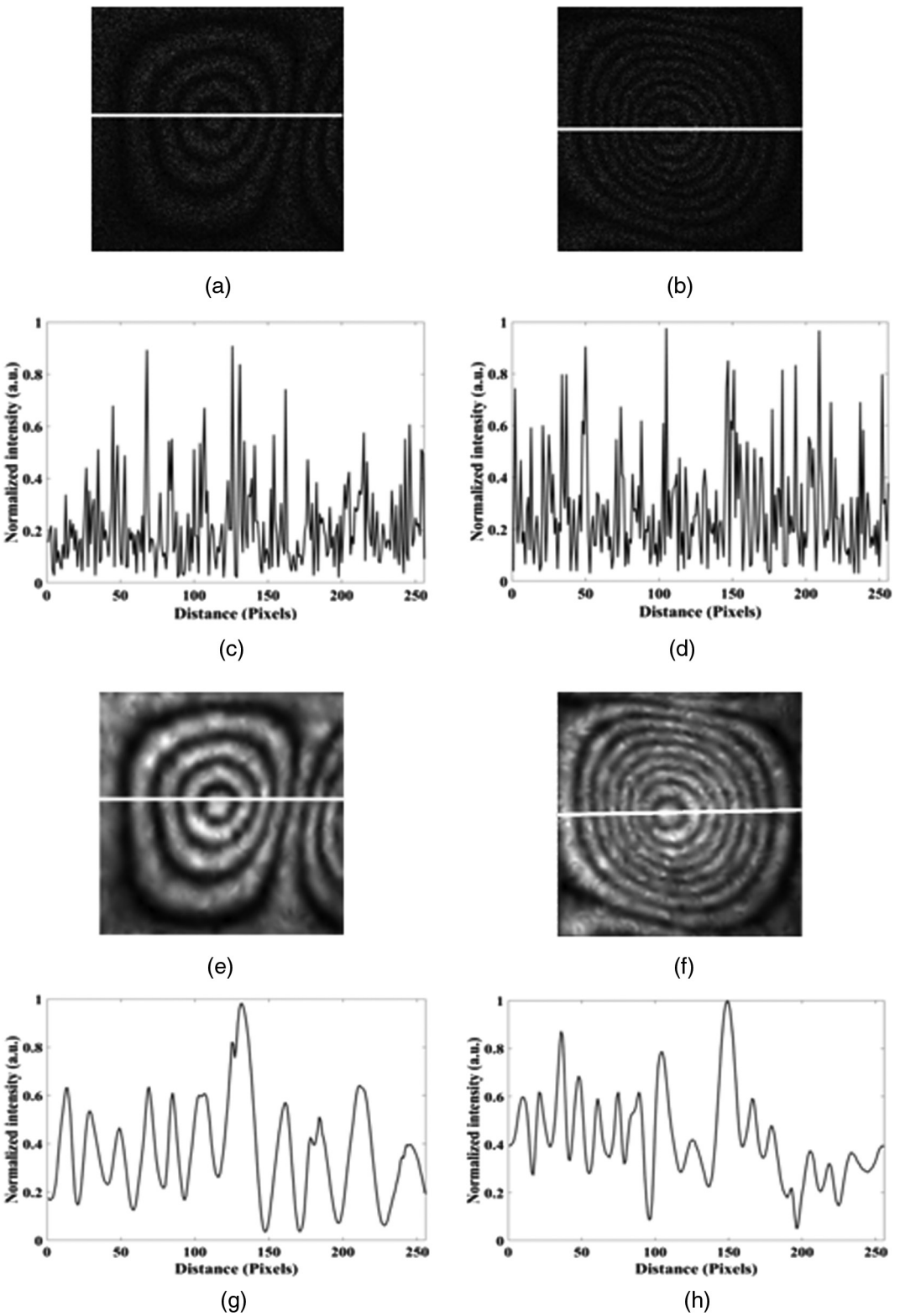

Fig. 13 (a) and (b) Experimental DSPI fringe patterns, (c) and (d) normalized intensity profile, (e) and (f) filtered DSPI fringes by the proposed method, and (g) and (h) corresponding normalized intensity profiles.

References

1. J. N. Butters and J. A. Leendertz, "Speckle pattern and holographic techniques in engineeringmetrology," *Opt. Laser Technol.* **3**(1), 26–30 (1971).
2. C. Wykes, "Use of electronic speckle pattern interferometry (ESPI) in the measurement of static and dynamic surface displacements," *Opt. Eng.* **21**(3), 213400 (1982).
3. K. Creath and G. Å. Slettemoen, "Vibration-observation techniques for digital speckle-pattern interferometry," *J. Opt. Soc. Am. A* **2**(10), 1629–1636 (1985).
4. F. Chen, C. T. Griffen, and T. E. Allen, "Digital speckle interferometry: some developments and applications for vibration measurement in the automotive industry," *Opt. Eng.* **37**(5), 1390–1398 (1998).
5. M. Kumar, K. K. Gaur, and C. Shakher, "Measurement of material constants (Young's modulus and Poisson's ratio) of polypropylene using digital speckle pattern interferometry (DSPI)," *J. Jpn. Soc. Exp. Mech.* **15**(Special Issue), s87–s91 (2015).
6. M. Kumar and C. Shakher, "Measurement of temperature and temperature distribution in gaseous flames by digital speckle pattern shearing interferometry using holographic optical element," *Opt. Lasers Eng.* **73**, 33–39 (2015).
7. M. Kumar, G. S. Khan, and C. Shakher, "Measurement of elastic and thermal properties of composite materials using digital speckle pattern interferometry," *Proc. SPIE* **9660**, 966011 (2015).
8. M. Kumar et al., "Measurement of strain distribution in cortical bone around miniscrew implants used for orthodontic anchorage using digital speckle pattern interferometry," *Opt. Eng.* **55**(5), 054101 (2016).
9. J. W. Goodman, "Statistical properties of laser speckle patterns," in *Laser Speckle and Related Phenomena*, J. C. Dainty, Ed., pp. 9–75, Springer, Berlin, Heidelberg (1975).
10. J. S. Lim and H. Nawab, "Techniques for speckle noise removal," *Opt. Eng.* **20**(3), 203472 (1981).
11. P. Varman and C. Wykes, "Smoothing of speckle and Moire fringes by computer processing," *Opt. Lasers Eng.* **3**(2), 87–100 (1982).
12. C. Tang, L. Wang, and H. Yan, "Overview of anisotropic filtering methods based on partial differential equations for electronic speckle pattern interferometry," *Appl. Opt.* **51**(20), 4916–4926 (2012).
13. M. B. Bernini, A. Federico, and G. H. Kaufmann, "Denoising of digital speckle pattern interferometry fringes by means of bidimensional empirical mode decomposition," *Proc. SPIE* **7063**, 70630D (2008).
14. J. Lee, "Digital image enhancement and noise filtering by use of local statistics," *IEEE Trans. Pattern Anal. Mach. Intell.* **PAMI-2**(2), 165–168 (1980).
15. C. Tomasi and R. Manduchi, "Bilateral filtering for gray and color images," in *Sixth Int. Conf. Comput. Vision (IEEE Cat. No. 98CH36271)*, pp. 839–846 (1998).
16. V. S. Frost et al., "A model for radar images and its application to adaptive digital filtering of multiplicative noise," *IEEE Trans. Pattern Anal. Mach. Intell.* **PAMI-4**(2), 157–166 (1982).
17. Y. Tounsi et al., "Speckle noise reduction in digital speckle pattern interferometric fringes by nonlocal means and its related adaptive kernel-based methods," *Appl. Opt.* **57**(27), 7681–7690 (2018).
18. S. G. Mallat, "A theory for multiresolution signal decomposition: the wavelet representation," *IEEE Trans. Pattern Anal. Mach. Intell.* **11**(7), 674–693 (1989).
19. C. Shakher et al., "Application of wavelet filtering for vibration analysis using digital speckle pattern interferometery," *Opt. Eng.* **41**(1), 176–181 (2002).
20. E. M. Barj et al., "Speckle correlation fringes denoising using stationary wavelet transform. Application in the wavelet phase evaluation technique," *Opt. Laser Technol.* **38**(7), 506–511 (2006).
21. Y. Tounsi, A. Siari, and A. Nassim, "Speckle noise reduction in digital speckle pattern interferometry using Riesz wavelets transform," in *Int. Conf. Adv. Technol. Signal and Image Process. (ATSIP)*, pp. 1–4 (2017).
22. G. H. Kaufmann and G. E. Galizzi, "Speckle noise reduction in television holography fringes using wavelet thresholding," *Opt. Eng.* **35**(1), 9–15 (1996).
23. P. Memmolo et al., "Quantitative phase maps denoising of long holographic sequences by using SPADEDH algorithm," *Appl. Opt.* **52**(7), 1453–1460 (2013).
24. S. Montresor and P. Picart, "Quantitative appraisal for noise reduction in digital holographic phase imaging," *Opt. Express* **24**(13), 14322–14343 (2016).
25. Q. Xiao, J. Li, and Z. Zeng, "A denoising scheme for DSPI phase based on improved variational mode decomposition," *Mech. Syst. Sig. Process.* **110**, 28–41 (2018).
26. M. Unser, D. Sage, and D. V. D. Ville, "Multiresolution monogenic signal analysis using the Riesz–Laplace wavelet transform," *IEEE Trans. Image Process.* **18**(11), 2402–2418 (2009).
27. E. M. Stein and G. Weiss, *Introduction to Fourier Analysis on Euclidean Spaces (PMS-32)*, Princeton University Press, Princeton, New Jersey (1971).
28. M. Unser and N. Chenouard, "A unifying parametric framework for 2D steerable wavelet transforms," *SIAM J. Imaging Sci.* **6**(1), 102–135 (2013).
29. D. Gabor, "Theory of communication. Part 1: The analysis of information," *J. Inst. Electr. Eng. Part III* **93**(26), 429–441 (1946).
30. M. Felsberg and G. Sommer, "The monogenic signal," *IEEE Trans. Signal Process.* **49**(12), 3136–3144 (2001).
31. M. Kumar et al., "Experimental investigation on butane diffusion flames under the influence of magnetic field by using digital speckle pattern interferometry," *Appl. Opt.* **54**(9), 2450–2460 (2015).
32. A. M. Eskicioglu and P. S. Fisher, "Image quality measures and their performance," *IEEE Trans. Commun.* **43**(12), 2959–2965 (1995).
33. Z. Wang and A. C. Bovik, "A universal image quality index," *IEEE Signal Process. Lett.* **9**(3), 81–84 (2002).

Sara Zada received her MSc degree in physics from Chouaib Doukkali University in 2010 and her PhD in applied optics from the same university in 2018. Her research includes the exploitation of empirical mode decomposition and monogenic signal in speckle interferometry.

Yassine Tounsi received his MSc degree in physics in 2015. He is a PhD student in applied optics at Chouaib Doukkali University. His current research interest includes speckle metrology, image denoising, and photoelasticimetry technique. He is a reviewer of the Applied Optics Journal.

Manoj Kumar received his BSc (Hons.) and MSc degrees in physics from the University of Delhi in 2006 and 2008, respectively, his MTech degree in instrumentation from the National Institute of Technology Kurukshetra in 2011, and his PhD in optical engineering from the Indian Institute of Technology Delhi, New Delhi, India, in 2016. He was a postdoctoral research fellow in the Department of Electrical and Computer Engineering at Ben-Gurion University of the Negev, Beer-Sheva, Israel. Presently, he is a JSPS postdoctoral research fellow at Kobe University, Japan. His research interests include 3-D imaging, biomedical optics, digital holography, and speckle metrology. He is a member of the Optical Society of America.

Fernando Mendoza-Santoyo is a former general director of Centro de Investigaciones en Optica, A.C., (CIO), León, Mexico. He has held positions in the USA and Europe as a visiting professor conducting research in electron holography and optical no destructive techniques applied to innovative nanomaterials and a wide variety of bio materials. He is currently in the board of editors of optics and lasers in engineering (Elsevier), and a topical editor for *Applied Optics*. He is an SPIE fellow and a member of its board of directors. Currently, he is an emeritus professor at CIO.

Abdelkrim Nassim received his PhD in physics from Chouaib Doukkali University, Morocco, in collaboration with FIAM Laboratory, Catholic University of Louvain, Belgium. During his research career, he published several papers about speckle interferometry technique in the two principal domains: speckle denoising and optical phase extraction. He is also a reviewer for JOLT journal (optics and laser technology). He has the skills and expertise in speckle interferometry, wavelet transform, and bidimensional empirical mode decomposition.